

# Modified Von Karman Trefftz Transformation with Computation of Aerodynamic Coefficients

Toufik Yahiaoui\* and Toufik Zebbiche\*

**Keywords** : Critical Points, Von Karman Trefftz Transformation, Joukowski Transformation, Circle, Ellipse, Airfoils, Trailing Edge angle, Cubic spline interpolation, Stretching function, Aerodynamics coefficients, Subsonic flow, Panels method

## ABSTRACT

The aim of this work is to develop a numerical calculation program to generate new airfoils geometries using a modified conformal transformation of the Von Karman Trefftz type from an ellipse, and by the consideration of the nonzero trailing edge angle, as a generalization of the classical transformations using a circle. The numerical calculation is defined by a new method based on the consideration of the transformation of a triangle connecting the two critical points with the point on the ellipse boundary, giving a single image in the airfoil plane. This is for each selected boundary point of the ellipse. Nodes condensation is used to refine the points in the neighbourhood of the leading edge region, in order to ensure its curvature. The determination of the maximum thickness value is presented. In this case, the interpolation of the coordinates of the airfoil points is made by the cubic spline interpolation. Normalization of the airfoil geometry is performed to reduce its size to the standard shape having a chord equal to unity. Infinity of shape of the airfoils is obtained by the variation of the trailing edge angle, the abscissa and the ordinate of the ellipse center, and the ratio of the ellipse radii's. The second part of the developed program consists in determining the aerodynamic pressure drag, lift and pitching moment coefficients of a subsonic flow around the generated airfoils by the panel method, with a comparison to the classic Von Karman airfoils.

## INTRODUCTION

The design of the airfoils plays an important role in the aerospace construction, to generate qualities on the aerodynamic forces according to our need. During 70 years of research from 1950 to the present, the development of the airfoils geometries has gone through several stages. Each designated airfoil has its own physical and aerodynamic characteristics.

*Paper Received April, 2023. Revised May, 2023. Accepted June, 2023. Author for Correspondence: Toufik Zebbiche.  
Email: z\_toufik270169@yahoo.fr*

*\*Professor, Institute of Aeronautics and Space Studies, University of Blida 1, BP 270 Blida 09000, Algeria.*

There are several types of airfoils, applied in subsonic Anderson (2007), Ashley and Landahl (1985), Katz and Plotkin (2015), Paraschivou (1998), and for supersonic regimes Fletcher (1988) and Ryhming (2010). Similarly, we have theoretical and experimental airfoils Abbott and Doenhoff (1959) and UIUC Applied Aerodynamic group (2013) and. First, the airfoils are generated by the conformal transformations Nehari (1982, and using the complex number functions Bruno (2019) and Gurlebeck and Morais (2008) by the *circle* transformation into an airfoil. Conformal transformations take critical points, which must be placed into the airfoil surface. So to generate an airfoil, we need a circle and a transformation with critical points.

We can cite the first basic Joukowski transformation Almeida and Malonek (2008) and Malonek and Almeida (2010). It uses two critical points and a circle. The main disadvantage of this transformation is that the generated airfoils have an angle at the *TE* equal to zero, which does not fall in agreement with reality, where all the airfoils have an angle different from zero at the *TE* Abbott and Doenhoff (1959) and UIUC Aerodynamic group (2013).

A generalization of this transformation is made by Von misses by considering always a circle, but with a number of critical points greater than two Barran and Hakuri (1991) and Hakuri (1987). The generated airfoils always have a *TE* angle equal to zero, which contradicts the reality. The resolution of this problem is made by Von Karma Trefftz who took an angle at the *TE* different from zero. Said transformation always uses a circle and two critical points Hakuri (1987) and Ryhming (2010).

The use of the complex numbers is necessary to determine the image of the circle by the conformal transformation Anderson (2007) and Bruno (2019). Functions based on complex numbers are multi vocal functions; it has several images from each point of the circle plane to the airfoil plane. This property makes the computational procedure very difficult to implement a numerical method in this context. Then the Joukovski transformation gives, for each point of the circle plane, two images in the airfoil plane. For the transformation of Von Karman Trefftz gives infinity of images. The Von Karman Trefftz transformation has four parameters, which are the angle of *TE*, position of *TE* critical point, abscissa and ordinate of the circle center. The quality of the generated airfoils requires an improvement to the needs of aerodynamic calculation. So, it requires the generation of other airfoils with several parameters.

There are other airfoils witch are generated by wind tunnel tests based on the aerodynamic calculations, and the shapes of the airfoils of different birds in nature. One

can find a series of airfoils developed experimentally adopting by several aerospace companies Abbott and Doenhoff (1959) and UIUC Applied Aerodynamic group (2013). If we consider a transformation to determine the inverse image of the experimental airfoil towards the original plane by Von Karaman Treftz transformation, we will find that the geometry becomes a pseudo circle, and not a perfect circle. This method is generally suitable for generating a curvilinear mesh around an airfoil to help solve the Euler or Navier Stocks equations.

The purpose of this work consists in carrying out a numerical calculation program making it possible to generate new airfoils geometries by using the conformal transformation of the Von Karman Treftz from an *ellipse* and not from a circle, and also by considering a nonzero *TE* angle, as a generalization of the classical transformations using a circle. The numerical calculation is defined by a new discretization method based on the consideration of a triangle connecting the two critical points with the ellipse boundary, giving a unique and the corresponding physical accepted image in the airfoil plane, for each selected point on the ellipse boundary. Nodes condensation is used to refine the points in the neighbourhood of the *LE* region, in order to ensure the rounding of this region. The determination of the maximum thickness value is presented. In this case, the interpolation of the coordinates of the airfoil points is necessary to obtain an analytical function to the extrados and the intrados of the airfoil. The cubic spline method is chosen in our study. The normalization of the airfoil geometry is carried out, in order to reduce its size to the standard shape having a chord equal to unity. An infinity of shape of the airfoils can be obtained by the variation of the *TE* angle, of the abscissa and the ordinate of the ellipse center, the position of the *TE* critical point, and the *ratio of the ellipse radii*'. The second part of the developed program consists in determining the aerodynamic drag, lift and pitching moment coefficients of a subsonic flow around the generated airfoils by the panel method, with a comparison to the classic Von Karman Treftz airfoils.

### PRESENTATION OF THE TRANSFORMATION

Consider the following Von Karman Treftz transformation for two critical points:

$$\frac{z - z_2}{z - z_1} = \left( \frac{\zeta - 1}{\zeta + 1} \right)^n \quad (1)$$

With:

$$n = 2 - \frac{\tau}{\pi} \quad (2)$$

The relation (1) allowing to transform a chosen ellipse into an airfoil as shown in the following figure 1.

The airfoil plane is denoted by  $z=x + j y$ , and the ellipse plane is denoted by  $\zeta = \zeta + j \eta$ .

We present the various necessary relations to transform an ellipse into an airfoil according to the figure 1. From the figure 1, we can write:

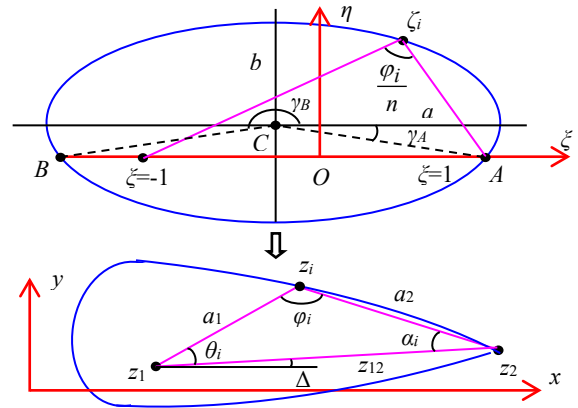


Figure 1. Transformation from an ellipse to an airfoil

The airfoil plane is denoted by  $z=x + j y$ , and the ellipse plane is denoted by  $\zeta = \zeta + j \eta$ .

We present the various necessary relations to transform an ellipse into an airfoil according to the figure 1. From the figure 1, we can write:

$$\varphi = \arg\left(\frac{z - z_2}{z - z_1}\right) = n \arg\left(\frac{\zeta - 1}{\zeta + 1}\right) \quad (3)$$

$$a_1 = |z - z_1| \quad (4)$$

$$a_2 = |z - z_2| \quad (5)$$

$$a_{12} = |z_1 - z_2| \quad (6)$$

$$\theta = \hat{z_2 z_1 z} \quad (7)$$

$$\alpha = \hat{z z_2 z_1} \quad (8)$$

In the triangle  $z_2 z_1 z$  of the figure 1, we have:

$$\varphi + \alpha + \theta = \pi \quad (9)$$

$$\frac{\sin \theta}{a_2} = \frac{\sin \varphi}{a_{12}} \quad (10)$$

$$\frac{\sin \alpha}{a_1} = \frac{\sin \varphi}{a_{12}} \quad (11)$$

According to the relation (1), we can write:

$$\lambda = \left| \frac{\zeta - 1}{\zeta + 1} \right|^n = \left| \frac{z - z_2}{z - z_1} \right| \quad (12)$$

And

$$\mu = \frac{b}{a} \quad (13)$$

The equation of the ellipse in the figure 1 is written:

$$\left( \frac{\zeta - \zeta_C}{a} \right)^2 + \left( \frac{\eta - \eta_C}{b} \right)^2 = 1 \quad (14)$$

The coordinates of the *TE* point are given by:

$$\xi_A = 1.00 \quad , \quad \eta_A = 0.0 \quad (15)$$

The radius  $a$  of the ellipse can be calculated by replacing (15) and the value of  $b$  of (13) into (14). After rearrangement we obtain the following result:

$$a = \sqrt{(\xi_C - 1)^2 + \left(\frac{\eta_C}{\mu}\right)^2} \quad (16)$$

The radius value  $b$  can be obtained from (13). The position of the point  $B$  in the ellipse plane can be calculated by replacing  $\xi = \xi_B$  and  $\eta = \eta_B = 0$ , as well as, the relation (16) in (14), we obtain:

$$\xi_B = -1 + 2\xi_C \quad (17)$$

Angles  $\gamma_A$  and  $\gamma_B$  made by the segments connecting the ellipse center  $C$ , and respectively the point  $A$  and  $B$ , presented in the figure 1, can be calculated by:

$$\gamma_A = a \tan\left(\frac{\eta_C}{\xi_A - \xi_C}\right) \quad (18)$$

$$\gamma_B = a \tan\left(\frac{\eta_C}{\xi_B - \xi_C}\right) \quad (19)$$

The value of  $a_{12}$  in the figure 1 can be calculated by the following relationship

$$a_{12} = \sqrt{(x_2 - x_1)^2 + (y_2 - y_1)^2} \quad (20)$$

## CALCULATION PROCEDURE

Consider the discretization of the ellipse boundary by  $m$  points. First, the angle  $\beta_i$  ( $i=1, 2, \dots, m$ ) must be determined as shown in the figure 2.

A node condensation is made in the region of the  $LE$  vicinity  $A$ , in order to ensure the airfoil curvature in this region. The condensation is given by Vinokur (1983):

$$s_i = Q_1 \eta_i^* + (1 - Q_1) \left[ 1 - \frac{\tanh[Q_2(1 - \eta_i^*)]}{\tanh(Q_2)} \right] \quad (21)$$

### For extrados

For the extrados region, the numbering of the nodes is counter clockwise, starting from the point  $A$ . Then point  $i=1$  coincides with the point  $A$ , and the point  $i=m_E$  coincides with the point  $B$ . So:

$$\eta_i^* = \frac{i-1}{m_E-1} \quad i=1, 2, \dots, m_E \quad (22)$$

Replacing (22) into (21), then substitute the obtained result in the following relation (23), we obtain the angle  $\beta_i$ , with condensation in the extrados region by the following relation

$$\delta_i = \gamma_A + s_i (\gamma_B - \gamma_A) \quad (23)$$

It is necessary to take the values of  $Q_1$  lower than 1.0 ( $Q_1=0.10$  for example) to condense the nodes towards the point  $B$ . The value of  $Q_2=2.00$ .

### For intrados

For the intrados region, the numbering of the nodes is counter clockwise, starting from the point  $B$ . Then,

the point  $i=m_E+1$  coincides with the point  $B$ , and the point  $i=m$  coincides with the point  $A$ . So:

$$\eta_i^* = \frac{i - m_E - 1}{m - m_E - 1} \quad i = m_E + 1, m_E + 2, \dots, m \quad (24)$$

Replacing (24) into (21), then substitute the obtained result in the following relation (25), we obtain the angle  $\beta_i$ , with condensation in the intrados region by:

$$\delta_i = \gamma_B + s_i (2\pi + \gamma_A - \gamma_B) \quad (25)$$

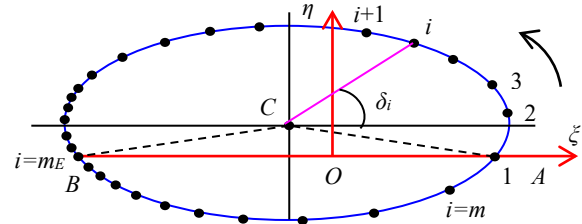


Figure 2. Discretization of the ellipse boundary and illustration of the angle  $\delta_i$

In this case, it is necessary to take values of  $Q_1$  superior to 1.0 ( $Q_1=1.90$  for example) to condense the nodes towards the point  $B$ . The value of  $Q_2=2.00$ .

Therefore the position of the point  $\zeta_i$  on the ellipse boundary as shown in the figure 1 is given by:

$$\begin{cases} \xi_i = \xi_C + a \cos \delta_i \\ \eta_i = \eta_C + b \sin \delta_i \end{cases}, \quad (i=1, 2, \dots, m) \quad (26)$$

According to (9), we can write for the point number  $i$ , the following relation:

$$\alpha_i = \pi - (\varphi_i + \theta_i) \quad (27)$$

Then from Merzbach and Boyer (2011)

$$\sin \alpha_i = \sin (\varphi_i + \theta_i) \quad (28)$$

Substituting (4) and (5) into (12), we obtain, for the point  $i$ , the following expression:

$$\lambda_i = \frac{a_2}{a_1} \quad (29)$$

Write  $a_1$  and  $a_2$  in terms of the other terms, respectively, from (11) and (10), then substitute the obtained results in (29), we obtain the following relation:

$$\frac{\sin (\varphi_i + \theta_i)}{\sin \theta_i} = \frac{1}{\lambda_i} \quad (30)$$

After rearrangement, the relation (30) becomes

$$\theta_i = a \tan\left(\frac{\lambda_i \sin \varphi_i}{1 - \lambda_i \cos \varphi_i}\right) \quad (31)$$

If the angle  $\theta_i < 0.0$ , we need the correction by  $\theta_i = \theta_i + \pi$ .

The calculation then consists of calculating the values of  $\varphi_i$  and  $\lambda_i$  for each value of  $(\xi_i, \eta_i)$  ( $i=1, 2, \dots, m$ ) given by (26). According to (12), we have:

$$\lambda_i = \left[ \frac{(\xi_i - 1)^2 + (\eta_i)^2}{(\xi_i + 1)^2 + (\eta_i)^2} \right]^{\frac{n}{2}} \quad (32)$$

According to the figure 1, the angle  $\varphi_i$  can be determined by the following relationship

$$\varphi_i = \left| \operatorname{atan}\left(\frac{\eta_i}{\xi_i - 1}\right) - \operatorname{atan}\left(\frac{\eta_i}{\xi_i + 1}\right) \right| \quad (33)$$

From (11) and (28), we can write:

$$(a_1)_i = a_{12} \frac{\sin(\varphi_i + \theta_i)}{\sin \varphi_i} \quad (34)$$

The angle  $\Delta$  in the figure 1 is calculated by:

$$\Delta = \operatorname{atan}\left(\frac{y_2 - y_1}{x_2 - x_1}\right) \quad (35)$$

Finally the position of the point  $z_i(x_i, y_i)$  on the airfoil boundary is calculated by the following relations.

For the extrados, we have

$$\delta_i \leq \gamma_B \quad (i=1, 2, \dots, m) \quad (36)$$

$$(x_E)_i = x_1 + a_1 \cos(\theta_i + \Delta) \quad (37)$$

$$(y_E)_i = y_1 + a_1 \sin(\theta_i + \Delta) \quad (38)$$

The number of points verifying the condition (36) is equal to  $m_E < m$ .

For the intrados, we have

$$\gamma_B \leq \delta_i \leq \gamma_A + 2\pi \quad (i=1, 2, \dots, m) \quad (39)$$

$$(x_I)_i = x_1 + a_1 \cos(\theta_i + \Delta) \quad (40)$$

$$(y_I)_i = y_1 - a_1 \sin(\theta_i + \Delta) \quad (41)$$

The number of points verifying the condition (39) is equal to  $m_I < m$ .

Points  $A$  and  $B$  and these images are counted for both extrados and intrados sides.

The position of the  $LE$  (point  $B$ ) can be calculated by replacing  $i=m_E$  in the relations (34) and (35).

For a standard presentation of the positions of the airfoil points, it is necessary to number the points of the extrados going from  $LE$  to  $TE$ .

Point  $B$  then becomes the first point for the extrados and the intrados

The airfoil chord is calculated as the distance between the critical point 2 and the  $LE$  point  $B$  by

$$C = x_2 - x_B \quad (42)$$

Usually we take the position of the critical points  $z_1$  and  $z_2$  on the horizontal axis to obtain the airfoil geometry. So  $y_1=y_2=0.0$ . It is recommended to translate the airfoil in such a way that the  $LE$  becomes at the point  $(0, 0)$ .

The obtained airfoil has a chord different to unity. So to obtain a standard geometry, the airfoil must be reduced by homothetic, so that its chord will be equal to unity.

Finally, the value of the maximum thickness is evaluated. In this case, the determined points by the conformal transformation are interpolated by the cubic spline method, in order, to find an analytical function on each side of the extrados and the intrados Wang (2011) and Suenaga and Sakai (2001). The dichotomy method is used again to determine the value of  $t_{\max}/C$  (%)

Demidowitch and Marron (1987) and Ralston and Rabinowitz (1985).

## AERODYNAMIC CALCULATION

The determination of the coefficients  $C_D$ ,  $C_L$  and  $C_M$  of a subsonic flow is interesting to evaluate the practical interest of the generated airfoils by the presented transformation. It is not necessary to calculate the flow around the original ellipse, and then transform the flow results into the airfoil plane. Direct determination of the flow in the airfoil plane is possible. Among several existing methods in the literature, the panel method is used Anderson (2007), Ashley and Landahl (1985), Katz and Plotkin (2015), Paraschivou (1998), and for supersonic regimes Fletcher (1988) and Ryhming (2010) and presented below. The purpose of the aerodynamic calculation is to test and use the generated airfoils in this study as typical applications. We are interested in the determination of the variation of the pressure ratio  $P/P_0$ , as well as, the Mach number on the extrados and the intrados airfoils surface, and deduce the associated aerodynamics coefficients. The calculation of  $C_M$  is made in relation to the airfoil  $LE$ .

Figure 3 represents a typical mesh on the airfoil boundary generated by our transformation; which is necessary for the calculation by the panel method.

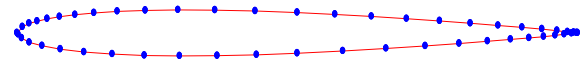


Figure 3. Typical mesh on the generated airfoil boundary

Figure 4 illustrates a typical segment of the discretization of the figure 3, and presents the notation and parameters related to segment  $(i)$ .

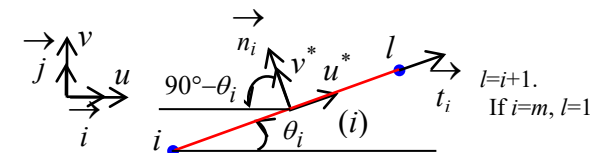


Figure 4. Scoring and system related to segment  $(i)$ .

The control points are located at the centers of the segments; their coordinates are therefore given by:

$$\begin{cases} g_i = \frac{x_i + x_l}{2} & l=i+1. \text{ If } i=m, l=1 \\ h_i = \frac{y_i + y_l}{2} & (i=1, 2, \dots, m) \end{cases} \quad (43)$$

The flow modelling is done by a distribution of the sources and vortices on each segment at the level of the control points, such that the vortex intensity is constant on all the segments, and that the intensity of the sources varies from one segment to another.

The components of the velocity  $V$  at each control point  $i$  are given by:

$$\begin{cases} u_i = u(g_i, h_i) \\ v_i = v(g_i, h_i) \end{cases} \quad i=1, 2, \dots, m \quad (44)$$

The slip condition means that the velocity is tangential to the wall, since the flow is of an in viscid ideal gas, and therefore the velocity normal to the surface of each segment is zero. From the figure 4, we can write

$$\vec{n}_i = -\sin \theta_i \vec{i} + \cos \theta_i \vec{j} \quad i=1, 2, \dots, m \quad (45)$$

The speed at control point  $i$  is expressed by:

$$\vec{V}_i = u_i \vec{i} + v_i \vec{j} \quad i=1, 2, \dots, m \quad (46)$$

The slip condition results in the fact that the scalar product  $\vec{V}_i \cdot \vec{n}_i = 0$ , whose application point is the control point  $i$ . This allows us to have, after mathematical development, the following expression:

$$-u_i \sin \theta_i + v_i \cos \theta_i = 0 \quad i=1, 2, \dots, m \quad (47)$$

Kutta's condition states that the tangential velocities for the first and the last segment are equal in moduli but yet opposite in sign. Knowing that the tangential velocity at a control point  $i$  ( $i=1, 2, \dots, m$ ) is given by

$$V_i = u_i \cos \theta_i + v_i \sin \theta_i \quad (48)$$

The condition of Kutta applied therefore to the first and to the last segment, makes it possible to obtain the following expression:

$$V_1 = V_m \quad (49)$$

Resulting in

$$u_1 \cos \theta_1 + v_1 \sin \theta_1 = u_m \cos \theta_m + v_m \sin \theta_m \quad (50)$$

The mathematical development of the slip conditions (46), and the Kutta condition (50), leads us to the following system of equations (51). These unknowns are the intensities  $q_j$  ( $j=1, 2, \dots, m$ ) of the sources, as well as, the vortex intensity  $\Gamma$ . Then, the system (51) is of  $(m+1)$  unknowns based on an asymmetric and full matrix of order  $(m+1) \times (m+1)$ .

$$\begin{cases} \sum_{j=1}^m A_{i,j} q_j + A_{i,m+1} \Gamma = b_i \text{ for } i=1, 2, \dots, m \\ \sum_{j=1}^m A_{m+1,j} q_j + A_{m+1,m+1} \Gamma = b_{m+1} \text{ for } i=m+1 \end{cases} \quad (50)$$

We put

$$\begin{cases} (f_1)_{i,j} = \frac{1}{2\pi} \left[ \sin(\theta_i - \theta_j) \ln \frac{r_{i,l}}{r_{i,j}} + \cos(\theta_i - \theta_j) \beta_{i,j} \right] \\ (f_2)_{i,j} = \frac{1}{2\pi} \left[ \cos(\theta_i - \theta_j) \ln \frac{r_{i,l}}{r_{i,j}} - \sin(\theta_i - \theta_j) \beta_{i,j} \right] \end{cases}$$

$$l=j+1. \text{ If } j=m \text{ then } l=1, (i=1, \dots, m), (j=1, \dots, m) \quad (51)$$

Then

$$A_{i,j} = (f_1)_{i,j} \quad (i=1, 2, \dots, m), (j=1, 2, \dots, m) \quad (52)$$

$$A_{i,m+1} = \sum_{j=1}^m (f_2)_{i,j} \quad (i=1, 2, \dots, m) \quad (53)$$

$$A_{m+1,j} = -[(f_2)_{1,j} + (f_2)_{m,j}] \quad (j=1, 2, \dots, m) \quad (54)$$

$$A_{m+1,m+1} = \sum_{j=1}^m [(f_1)_{1,j} + (f_1)_{m,j}] \quad (55)$$

$$b_i = V_\infty \sin(\theta_i - \alpha) \quad i=1, 2, \dots, m \quad (56)$$

$$b_{m+1} = -V_\infty \cos(\theta_1 - \alpha) - V_\infty \cos(\theta_m - \alpha) \quad (57)$$

The angle  $\beta_{i,j}$  is defined according, to the figure 5, by the following relationship (58):

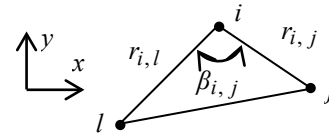


Figure 5. Angle illustration  $\beta_{i,j}$

$$\beta_{i,j} = \begin{cases} \operatorname{atan} \left( \frac{a_{i,j} b_{i,j} - c_{i,j} d_{i,j}}{c_{i,j} b_{i,j} + a_{i,j} d_{i,j}} \right) & \text{if } i \neq j \\ \pi & \text{if } i=j \end{cases} \quad \begin{matrix} l=j+1. \text{ If } j=m, l=1 \\ (i=1, 2, \dots, m) \\ (j=1, 2, \dots, m) \end{matrix} \quad (58)$$

With

$$\begin{cases} a_{i,j} = h_i - y_l \\ b_{i,j} = g_i - x_j \\ c_{i,j} = g_i - x_l \\ d_{i,j} = h_i - y_j \end{cases} \quad \begin{matrix} (i=1, 2, \dots, m) \\ (j=1, 2, \dots, m) \end{matrix} \quad (59)$$

The distance  $r_{i,j}$  is given by:

$$r_{i,j} = \sqrt{(x_j - g_i)^2 + (y_j - h_i)^2} \quad \begin{matrix} (i=1, 2, \dots, m) \\ (j=1, 2, \dots, m) \end{matrix} \quad (60)$$

The resolution of the system equation is made either by the direct Khalestski method,

The velocity  $V_i$  at points  $i$  ( $i=1, 2, \dots, m$ ) is given by:

$$V_i = V_\infty \cos(\theta_i - \alpha) - \sum_{j=1}^m q_j (f_2)_{i,j} + \Gamma \sum_{j=1}^m (f_1)_{i,j} \quad (i=1, 2, \dots, m) \quad (61)$$

The angle that segment number  $i$  ( $i=1, 2, \dots, m$ ) makes with the horizontal is given by:

$$\theta_i = \operatorname{atan} \left( \frac{y_l - y_i}{x_l - x_i} \right) \quad \begin{matrix} l=i+1. \text{ If } i=m, l=1 \\ (i=1, 2, \dots, m) \end{matrix} \quad (62)$$

The distance  $r_{i,j}$  connected between node  $j$  to control point  $i$  is given by (52).

The angle  $\beta_{i,j}$  for which we see segment number  $j$  at control point  $i$  is given by relation (60).

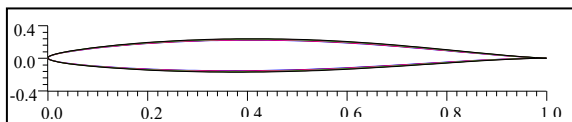
When we calculate the velocity at each point  $i$  by (53), the pressure ratio  $P/P_0$  can be determined by the Bernoulli equation Anderson (2007), Ashley and Landahl (1985), Katz and Plotkin (2015), Paraschivou

(1998), and for supersonic regimes Fletcher (1988) and Ryhming (2010). The aerodynamics coefficients  $C_D$ ,  $C_L$  and  $C_M$  can be obtained by standard formulae Anderson (2007), Ashley and Landahl (1985), Katz and Plotkin (2015), Paraschivou (1998), and for supersonic regimes Fletcher (1988) and Ryhming (2010).

### RESULTS AND COMMENTS

In this part, we will present the various obtained results by the developed numerical program. The airfoil geometry depends on four parameters which are the  $TE$  angle, the abscissa and the ordinate of the ellipse enter, and the ratio of the ellipse radii.

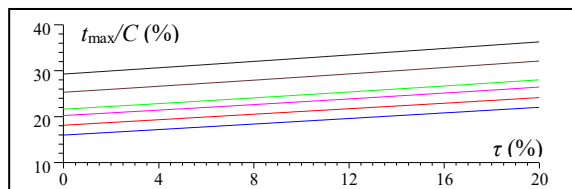
Figure 6 represents a typical example on the  $TE$  angle  $\tau$  effect on the obtained airfoil geometry for  $\tau=0^\circ, 2^\circ, 4^\circ, 6^\circ, 8^\circ$  and  $10^\circ$ . The other data such as the position of the ellipse center is taken equal to  $\zeta_c=-0.2$  and  $\eta_c=0.1$ . The ratio of the ellipse radii is taken to  $\mu=1.20$ . We clearly notice the effect of  $\tau$  on the airfoil shape. When  $\tau=0^\circ$  the airfoil does not become the Joukovski airfoil, since the transformation is not from a circle. In reality, we cannot perfectly build an airfoil with a  $TE$  angle equal to zero, which is interesting to take into consideration this angle during the transformation, hence the interest to have airfoils with a non-zero  $TE$  angle.



Curve (blue color):  $\tau=0^\circ$ . Curve (red color):  $\tau=2^\circ$   
 Curve (purple color):  $\tau=4^\circ$ . Curve (green color):  $\tau=6^\circ$   
 Curve (Brown Color):  $\tau=8^\circ$ . Curve (black color):  $\tau=10^\circ$

Figure 6. Effect of  $TE$  angle  $\tau$  on the airfoil geometry for  $m=300, \zeta_c=-0.2, \eta_c=0.1$  and  $\mu=1.20$

Figure 7 represents the variation of the maximum thickness obtained by our transformation as a function of the  $TE$  angle  $\tau$  for a some values of  $\mu$ . The data in this figure are  $\eta_c=0.2$  and  $\zeta_c=-0.2$ . We notice that the maximum thickness increases with the increase in the angle  $\tau$ , because there is airfoil opening at  $TE$  with increase in  $\tau$ , which will influence the airfoil curvature giving at the end an increase of the maximum thickness. Note that the more the ratio  $\mu$  increases progressively, there is an increase in the maximum thickness.



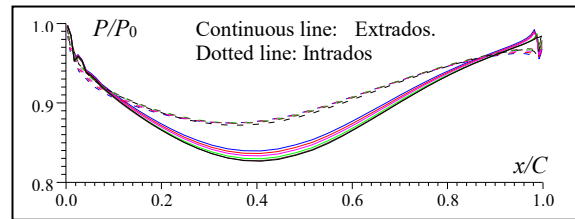
Curve (blue color):  $\mu=0.92$ . Curve (red color):  $\mu=0.95$   
 Curve (purple color):  $\mu=0.98$ . Curve (green color):  $\mu=1.00$   
 Curve (brown color):  $\mu=1.05$ . Curve (black color):  $\mu=1.10$

Figure 7. Variation of  $t_{max}/C$  with  $\tau$  for  $\zeta_c=-0.2$  and  $\eta_c=0.2$

The Von Karman Trefftz airfoil is obtained only by the value of  $\mu=1.00$  represented by the green curve in the figure 7. So if we want to obtain an airfoil with a very small thickness, it is recommended to take a value of  $\mu$

less than unity. So to have a large enough thickness, it is recommended to also take a large enough value of  $\mu$ . The Von Karman Trefftz airfoil does not necessarily give the best choices of recommended airfoil thickness. On the contrary, it only gives a single, non-disputable value. When  $\tau=0^\circ$ , the obtained airfoil is not the Joukovski airfoil, since the starting geometry is not taken as a circle.

Figure 8 represents the variation of  $P/P_0$  on the airfoil surface presented in the figure 6. The aerodynamic data taken in this example are  $M_\infty=0.3, T_0=300$  K,  $\alpha=0^\circ$  with air chosen as generator gas for external aerodynamics and ambient temperature. The example presented is for the case of subsonic flow. We used the panel method for the development of the numerical program. It is noticed that  $P/P_0$  changes with the shape of the obtained airfoil. For the Von Karman Trefftz airfoil, the variations are presented in the green color. The values of  $C_D, C_L$  and  $C_M$  associated with the example of the figure 7 are presented in the table 1. It should be noted that the calculated drag is only the drag due solely to the pressure. We notice that the  $C_D, C_L$  and  $C_M$  increase with the increase of  $\tau$ .



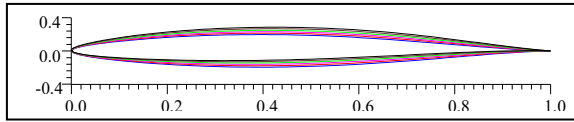
Curve (blue color):  $\tau=0^\circ$ . Curve (red color):  $\tau=2^\circ$   
 Curve (purple color):  $\tau=4^\circ$ . Curve (green color):  $\tau=6^\circ$   
 Curve (Brown color):  $\tau=8^\circ$ . Curve (black color):  $\tau=10^\circ$

Figure 8. Variation of  $P/P_0$  on the airfoil surface of the figure 6 for  $M_\infty=0.30, \alpha=0^\circ$ , air and  $T_0=300$  K.

Table 1.  $C_D, C_L$  and  $C_M$  of the airfoils of the figure 6

$\tau$ ( $^\circ$ )	$C_D$	$C_L$	$C_M$
0	-0.00331	0.23394	0.10966
2	-0.00233	0.27616	0.12927
4	-0.00152	0.31310	0.14644
6	-0.00002	0.36899	0.17224
8	0.00049	0.39365	0.18375
10	0.00152	0.41316	0.16955

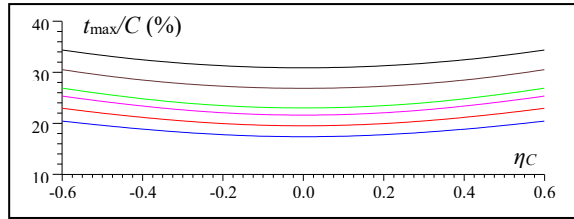
Figure 9 represents the effect of the ellipse ordinate center position  $\eta_c$  of the transformation on the geometry of the modified Von Karman Trefftz airfoil, considering the example for  $\tau=5^\circ$  and  $\zeta_c=0.20$ . The number of the taken discretization points equal to  $m=300$  with nodes condensation towards the  $LE$  region. The values of  $\eta_c$  are taken equal respectively to  $\eta_c=0.0, 0.05, 0.10, 0.15, 0.20$  and  $0.25$ . When one gradually increases the value of the ordinate  $\eta_c$  after a certain limit value, the use of the Von Karman Trefftz transformation gives a geometry which becomes more unsuitable to use as an airfoil in aerodynamic applications. Another parameter used to describe the obtained airfoils geometries is the airfoil camber. It is obtained as the average of the ordinate between the value of the extrados and the intrados. In this case, and according to the results of the figure 9, the increase in the ellipse ordinate increases the camber of the airfoil. Obtaining non-symmetrical airfoils is noticed in the figure 9.



Curve (blue color):  $\eta_C=0.0$ . Curve (red color):  $\eta_C=0.05$   
 Curve (purple color):  $\eta_C=0.10$ . Curve (green color):  $\eta_C=0.15$   
 Curve (brown color):  $\eta_C=0.20$ . Curve (black color):  $\eta_C=0.25$

Figure 9. Effect of the ordinate  $\eta_C$  of the ellipse center on the airfoil geometry for  $\tau=5^\circ$ ,  $\zeta_C=-0.20$  and  $\mu=1.20$

Figure 10 represents the variation of the maximum thickness as a function of the ordinate  $\eta_C$  for some values of  $\mu$ .



Curve (blue color):  $\mu=0.92$ . Curve (red color):  $\mu=0.95$   
 Curve (purple color):  $\mu=0.98$ . Curve (green color):  $\mu=1.00$   
 Curve (brown color):  $\mu=1.05$ . Curve (black color):  $\mu=1.10$

Figure 10. Variation of  $t_{max}/C$  with  $\eta_C$  for  $\zeta_C=-0.2$  and  $\tau=5^\circ$

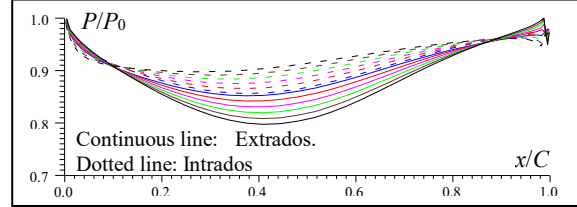
The data of this figure are  $\tau=5^\circ$  and  $\zeta_C=-0.2$ . We notice that we have symmetry on the airfoil shape with respect to the horizontal axis, since there is symmetry of the variation  $t_{max}$  with  $\eta_C$ . The maximum thickness increases with the increase in the ordinate  $\eta_C$ . The more the ratio  $\mu$  increases progressively, there is an increase in the maximum thickness. The Von Karman Treftz airfoil is obtained only by the value of  $\mu=1.00$  represented by the green curve in the figure 10.

If we want to obtain an airfoil with a very small thickness, it is recommended to take a lower value of  $\mu$ . So to have a large enough thickness, it is recommended to also take a large enough value of  $\mu$ . The Von Kar-man Treftz airfoil does not necessarily give the best choices of recommended airfoil thickness. On the contrary, it only gives a single, non-disputable value.

Figure 11 represents the variation of  $P/P_0$  on the surface of the airfoils presented in the figure 9. The aerodynamic data taken in this example are  $M_\infty=0.3$ ,  $T_0=300$  K and  $\alpha=0^\circ$  with air chosen as generator gas for external aerodynamics. We used the panel method for the development of the numerical programs. It is noticed on the variation of  $P/P_0$  changes with the shape of the obtained airfoils. For the Von Karman Treftz airfoil, the variations are presented with the green color. The aerodynamic coefficients  $C_D$ ,  $C_L$  and  $C_M$  associated with the example of the figure 9 are presented in the table 2. We note that these coefficients increase with the increase in  $\eta_C$ , which is interpreted by the size of the airfoil which becomes large enough with the increase in  $\eta_C$ .

Figure 12 represents the position effect of the ellipse abscissa  $\zeta_C$  of our transformation on the modified Von Karman Treftz airfoil geometry, considering the example for  $\tau=5^\circ$  and  $\eta_C=0.10$ . The number of the taken discretization point is equal to  $m=300$  with nodes condensation towards the LE region. The values of  $\zeta_C$  are

taken equal respectively to  $\zeta_C=0.0, -0.05, -0.10, -0.15, -0.20$  and  $-0.25$ . When one gradually increases the value of the abscissa  $\zeta_C$  after a certain limit value, the use of the transformation gives a geometry which becomes more unsuitable to use as an airfoil in the aerodynamic applications.



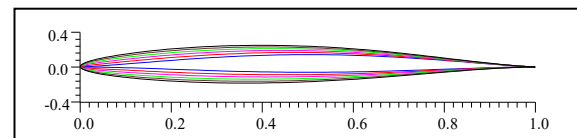
Curve (blue color):  $\eta_C=0.0$ . Curve (red color):  $\eta_C=0.05$   
 Curve (purple color):  $\eta_C=0.10$ . Curve (green color):  $\eta_C=0.15$   
 Curve (Brown color):  $\eta_C=0.20$ . Curve (black color):  $\eta_C=0.25$

Figure 11. Variation of  $P/P_0$  on the airfoils surface of the figure 9 for  $M_\infty=0.30$ ,  $\alpha=0^\circ$ , air and  $T_0=300$  K.

According to the results of the figure 12, the increase in the abscissa  $\zeta_C$  makes the increase in the camber of the airfoil. Non-symmetrical airfoils are noticed in the figure 12. It should be noted although to have airfoil geometry by the transformation, it is necessary to locate the ellipse center only in the second quadrant

Table 2.  $C_D$ ,  $C_L$  and  $C_M$  of the airfoils of the figure 11

$\eta_C$	$C_D$	$C_L$	$C_M$
0.00	0.00111	0.06991	0.03266
0.05	0.00114	0.20398	0.09522
0.10	0.00117	0.36051	0.16831
0.15	0.00313	0.50368	0.23551
0.20	0.00562	0.64142	0.30055
0.25	0.00860	0.77265	0.36302

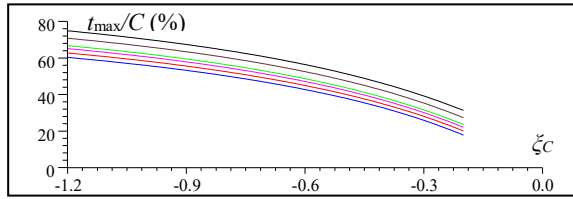


Curve (blue color):  $\zeta_C=-0.00$ . Curve (red color):  $\zeta_C=-0.05$   
 Curve (purple color):  $\zeta_C=-0.10$ . Curve (green color):  $\zeta_C=-0.15$   
 Curve (Color Brown):  $\zeta_C=-0.20$ . Curve (black color):  $\zeta_C=-0.25$

Figure 12. Effect of the abscissa  $\zeta_C$  on the airfoil geometry for  $\tau=5^\circ$ ,  $\eta_C=0.10$  and  $\mu=1.20$

Figure 13 represents the variation of the maximum thickness as a function of the abscissa  $\zeta_C$  for some values of  $\mu$ . The data of this figure are  $\tau=5^\circ$  and  $\eta_C=0.20$ . We notice an increase of the maximum thickness with the increase of  $\zeta_C$ , because there is a distance between the ellipse center and the reference mark center. The more the ratio  $\mu$  increases progressively, there is a very small change in an increase in the maximum thickness. The Von Karman Treftz airfoil is obtained only by the value of  $\mu=1.00$  represented by the green curve in the figure 13. So, to obtain an airfoil with a very small thickness, it is recommended to take a lower value of  $\mu$ . So to have a large thickness, it is also taking a large enough value of  $\mu$ .

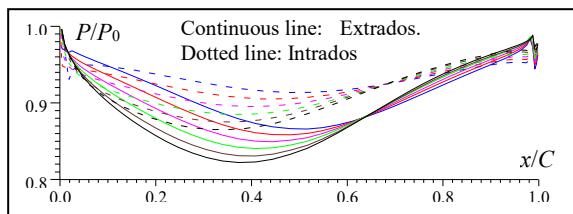
Figure 14 represents the variation of  $P/P_0$  on the surface of the airfoils of the figure 12.



Curve (blue color):  $\mu=0.92$ . Curve (red color):  $\mu=0.95$   
 Curve (purple color):  $\mu=0.98$ . Curve (green color):  $\mu=1.00$   
 Curve (brown color):  $\mu=1.05$ . Curve (black color):  $\mu=1.10$

Figure 13. Variation of  $t_{max}/C$  with  $\zeta_C$  for  $\eta_C=0.2$  and  $\tau=5^\circ$

The aerodynamic data taken for this example are  $M_\infty=0.3$ ,  $T_0=300$  K,  $\alpha=0^\circ$ . The panel method was used to calculate the aerodynamic coefficients  $C_D$ ,  $C_L$  and  $C_M$ . It is noticed on the variation of  $P/P_0$  with the shape of the obtained airfoils. For the Von Karman Trefftz airfoil, the variations are presented by green color. The aerodynamic coefficients associated of the example of the figure 9 are presented in the table 3. The  $C_D$ ,  $C_L$  and  $C_M$  increase with the increase in  $\zeta_C$ , giving large airfoil size



Curve (blue color):  $\zeta_C=-0.00$ . Curve (red color):  $\zeta_C=-0.05$   
 Curve (purple color):  $\zeta_C=-0.10$  Curve (green color):  $\zeta_C=-0.15$   
 Curve (Color Brown):  $\zeta_C=-0.20$ . Curve (black color):  $\zeta_C=-0.25$

Figure 14. Variation of  $P/P_0$  on the airfoils surface of the figure 12 for  $M_\infty=0.30$ ,  $\alpha=0^\circ$ , air and  $T_0=300$  K.

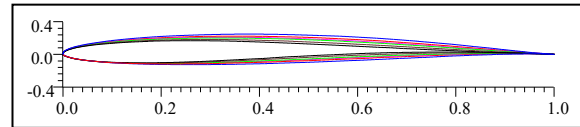
Table 3.  $C_D$ ,  $C_L$  and  $C_M$  of the airfoils of the figure 14

$\zeta_C$	$C_D$	$C_L$	$C_M$
0.00	0.00379	0.33599	0.16888
-0.05	0.00313	0.33818	0.16626
-0.10	0.00303	0.33824	0.16294
-0.15	0.00265	0.33710	0.15977
-0.20	0.00117	0.36051	0.16831
-0.25	0.00043	0.36603	0.16939

Figure 15 is the famous figure that represents the difference between our transformation and the classical Von Karman Trefftz transformation. So in this figure, we have varied the ratio  $\mu$  of the ellipse radius in the vicinity of  $\mu=1.00$ . For this latter value, we obtain purely the classical Von Karman Trefftz transformation when  $\tau \neq 0^\circ$ , and we obtain the Joukowski transformation when  $\tau=0^\circ$ . The number of the taken discretization points is equal to  $m=300$  with nodes condensation towards the LE region. The values of  $\mu$  are taken equal respectively to  $\mu=0.92$ , 0.95, 0.98, 1.00, 1.05 and 1.10. When, one gradually increases the value of  $\mu$  after a certain upper limit value, or decreases this value after a certain lower limit, the use of the modified Von Karman Trefftz transformation gives an airfoil geometry that becomes increasingly unsuitable to aerodynamic applications.

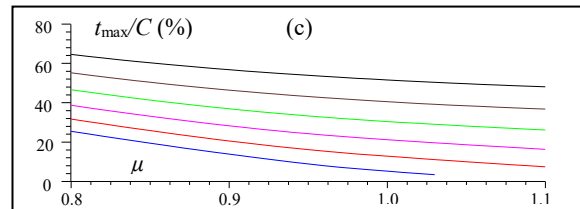
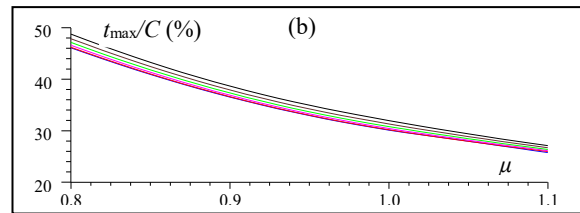
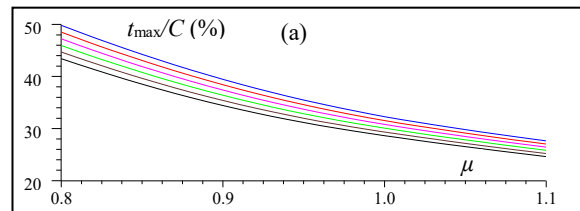
Figure 16 represents the variation of the maximum thickness of the obtained airfoils as a function of the ration  $\mu$ , respectively for the variation of  $\tau$  represented by figure 16(a), the variation of  $\eta_C$  represented by figure

16(b) and by the variation of  $\zeta_C$  represented by figure 16(c). We have not represented the variation of radius  $a$ , since it takes a single value with the variation of  $\mu$ . The maximum thickness decreases with the increase of  $\mu$ , because there is a closer proximity of the ellipse center towards the center of the reference mark. If one wants to obtain thick airfoils, it is necessary to take a value of  $\mu$  lower than the unit in the lower limit. The Von Karman Trefftz airfoil is obtained only by the value of  $\mu=1.00$  represented by the green curve in the figure 16.



Curve (blue color):  $\mu=0.92$ . Curve (red color):  $\mu=0.95$   
 Curve (purple color):  $\mu=0.98$ . Curve (green color):  $\mu=1.00$   
 Curve (brown color):  $\mu=1.05$ . Curve (black color):  $\mu=1.10$

Figure 15. Effect of  $\mu$  on airfoil geometry for  $\tau=5^\circ$ ,  $\zeta_C=-0.2$  and  $\eta_C=0.10$



(a): Distribution of  $\tau$  with  $\zeta_C=0.20$  and  $\eta_C=0.10$   
 (b): Distribution of  $\eta_C$  with  $\tau=5^\circ$  and  $\zeta_C=0.20$   
 (c): Distribution of  $\zeta_C$  with  $\tau=5^\circ$  and  $\eta_C=0.10$

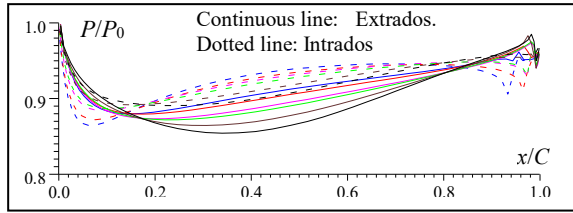
Curve (blue color): (a):  $\tau=0^\circ$ . (b):  $\eta_C=0.0$ , (c):  $\zeta_C=0.05$   
 Curve (red color): (a):  $\tau=2^\circ$ . (b):  $\eta_C=0.05$ , (c):  $\zeta_C=0.10$   
 Curve (purple color): (a):  $\tau=4^\circ$ . (b):  $\eta_C=0.10$ , (c):  $\zeta_C=-0.15$ .  
 Curve (green color): (a):  $\tau=6^\circ$ . (b):  $\eta_C=0.15$ , (c):  $\zeta_C=-0.20$ .  
 Curve (Brown color): (a):  $\tau=8^\circ$ . (b):  $\eta_C=0.20$ , (c):  $\zeta_C=-0.25$   
 Curve (black color): (a):  $\tau=10^\circ$ . (b):  $\eta_C=0.25$ , (c):  $\zeta_C=-0.30$

Figure 16. Variation of  $t_{max}/C$  (%) with  $\mu$

Figure 17 represents the variation of  $P/P_0$  on the airfoils surface of the figure 17. The aerodynamic data taken in this example are  $M_\infty=0.3$ ,  $T_0=300$  K,  $\alpha=0^\circ$  with air. The panel method was used to calculate the aerodynamic coefficients. It is noticed on the variation of  $P/P_0$  changes with the obtained airfoils shapes.

For the Von Karman Trefftz airfoil, the variations are presented with the green color. The aerodynamic coefficients associated with the example of the figure 15

are presented in the table 4. We note that these coefficients increase with the increase in  $\mu$ , that is to say for the thick airfoils. While for small values of  $\mu$ , which is the case for thin airfoils, one of the small values of  $C_D$ ,  $C_L$  and  $C_M$  was obtained, which is the case in reality.



Curve (blue color):  $\mu=0.92$ . Curve (red color):  $\mu=0.95$   
 Curve (purple color):  $\mu=0.98$ . Curve (green color):  $\mu=1.00$   
 Curve (brown color):  $\mu=1.05$ . Curve (black color):  $\mu=1.10$

Figure 17. Variation of  $P/P_0$  on the airfoils surface of the figure 16 for  $M_\infty=0.30$ ,  $\alpha=0^\circ$ , air and  $T_0=300$  K.

Table 4.  $C_D$ ,  $C_L$  and  $C_M$  of the airfoils in the figure 17

$\mu$	$C_D$	$C_L$	$C_M$
0.92	0.00116	0.12389	0.06585
0.95	0.00135	0.14099	0.14099
0.98	0.00171	0.28069	0.13078
1.00	0.00240	0.28367	0.13246
1.05	0.00271	0.32554	0.15269
1.10	0.00284	0.34323	0.16023

### VALIDATION WITH NUMERICAL AND EXPERIMENTAL STUDIES

The validation of the first part of the generation of the new generated airfoils geometries is done with the classic VonKarmn Trefftz and Joukowski airfoils according to Paraschivou (1998).

For the second part, the validation the numerical program and the comparison of our obtained results on the aerodynamic calculation is made for the NACA 0012, since it is frequently studied numerically according to Paraschivou (1998), and experimentally according to Elmaani and Radi (2019).

Tables 5 and 6 represent respectively a comparison of  $C_D$  and  $C_L$  between our results (1<sup>st</sup> column) and the numerical (2<sup>nd</sup> column) from Paraschivou (1998), experimental results (3<sup>rd</sup> column) from Elmaani and Radi (2019). No published values were found for the  $C_M$  coefficient. The results presented in those tables concern NACA 0012. We note that the error obtained by panel's method is small and acceptable error and witch can be justified by the physical phenomenon.

Table 5. Comparison of  $C_D$  for NACA 0012,  $M_\infty=0.3$

$\alpha$ ( $^\circ$ )	$C_D$ our results	$C_D$ from Paraschivou (1998)	$C_D$ from Elmaani and Radi (2019)
2	$13.5 \times 10^{-3}$	$0.68 \times 10^{-3}$	$23.4 \times 10^{-3}$
3	$17.5 \times 10^{-3}$	$0.71 \times 10^{-3}$	$23.8 \times 10^{-3}$
4	$22.9 \times 10^{-3}$	$0.75 \times 10^{-3}$	$24.5 \times 10^{-3}$

Table 6. Comparison of  $C_L$  for NACA 0012 when  $M_\infty=0.3$

$\alpha$ ( $^\circ$ )	$C_L$ our results	$C_L$ from Paraschivou (1998)	$C_L$ from Elmaani and Radi (2019)
2	0.268	0.238	0.220
3	0.342	0.358	0.330
4	0.443	0.478	0.440

Concerning the variation of  $P/P_0$  and  $C_D$ ,  $C_L$  and  $C_M$  as presented in the figures 9, 12, 15 and 18 and the tables 1, 2, 3 and 4, we note that the variation of  $P/P_0$  is very large in the vicinity of the  $LE$  and less for  $TE$  region. For this reason we used a mesh refinement in these two regions on the surface of the airfoils to have a good presentation of these two parameters. This large variation is due to the large variation in the vertical airfoil geometry in front of the flow, which is interpreted by the position of the maximum thickness in the vicinity of this region. Generally the position of the maximum thickness does not exceed about from 25% to 30%. The location of the maximum thickness at 25% up to 30% is recommended to allow the airfoil to penetrate the upstream medium with a large decrease in  $C_D$ . This condition is necessary for the airfoils of aircraft.

### CONCLUSIONS

We have developed a numerical calculation program that can determine airfoils geometries from an ellipse as a generalization of the Von Karman Trefftz transformation, with a calculation of the aerodynamic coefficients  $C_D$ ,  $C_L$  and  $C_M$  of a subsonic flow by the panel method. The following conclusions can be drawn:

The presented transformation is a generalization of those Von Karm Trefftz and Joukovski. Joukovski airfoils are obtained when  $\mu=1.00$  and  $\tau=0^\circ$ , and Von Karman Trefftz airfoils are obtained when  $\mu=1.00$  and  $\tau \neq 0.0$ .

The presented transformation depends on 5 parameters which are the  $TE$  airfoil angle, the ratio  $\mu$  of the ellipse radii, the abscissa and the ordinate of the ellipse center and the position of the  $TE$ . The results found are the airfoil geometry coordinates  $(x, y)$ , and its maximum thickness value.

To obtain small thickness, it is necessary to take the ratio  $\mu$  greater than unity or a value close to zero of  $\eta_c$ . However, a slight variation of  $t_{max}$  is obtained with the variation of  $\eta_c$ . When the value of  $\mu$  decreases, the airfoils become gradually thinner, and the coefficients  $C_D$ ,  $C_L$  and  $C_M$  also decrease, this falls in line with reality.

The standard airfoil shape is presented by normalizing its geometry to obtain a chord equal to 'unity, and a location in the interval  $[0, 1]$ .

The difference between the Von Karman Trefftz transformation and our transformation is that the latter gives a variety on the change of the maximum thickness and the airfoil camber by the variation of new parameter  $\mu$ , including the classical Von Karman Trefftz transformation allow giving a single unique value.

### FUTURE WORK

As future work, we can develop new airfoils based on the Von Karman Trefftz transformation but at three or several critical points generated always from an ellipse to determine airfoils with more parameters on the aerodynamic improvement calculation.

### REFERENCES

Abbott I. H. and von Doenhoff A. E., "Theory of wing sections: Including a summary of Airfoil data," Dover Publications, Inc., New York, Vol. II, (1959)

Almeida R. D. and Malonek H. R., "On a higher dimensional analogue of the Joukowski transformation," in Conference Proceedings, Vol. 1048, American Institute of Physics, New York, 2008, PP. 630–633. (2008)

Anderson, John D. "Fundamentals of Aerodynamics," 4<sup>th</sup> Edition. New York: McGrawHill, (2007)

Ashley H. and Landahl M., "Aerodynamics of Wing and Bodies," 2<sup>nd</sup> Edition, Dover Publication, (1985)

Barran, M., Hakuri, H., "On two new functional equations for generalized Joukowski transformations," Annales Polonici Mathematici, Vol. 56, PP. 79-85, (1991)

Bruno C., "L'application des nombres complexes au calcul des profils d'ailes," Comptes Rendus Mécanique, Vol. 347, PP. 544-549, (2019)

Demidovitch B. et Marron I., "Eléments de Calcul Numérique," Edition Mir, Moscou, (1987)

Elmaani R., Radi B. and Alhami A., "CFD Analysis and Shape Optimization of NACA0012 Airfoil for Different Mach Numbers," Proceedings of the 5<sup>th</sup> International Conference on Optimization and Applications (ICOA), (2019).

Fletcher C. A. J., "Computational Techniques for Fluid Dynamics: Specific Techniques for Different Flow Categories," Vol. II, Springer Verlag, Berlin, Heidelberg, Germany, (1988)

Gurlebeck K. and Morais, J., "Geometric characterization of M-conformal mappings," Proc. 3<sup>rd</sup> International Conference on Applied of Geometric Algebras in Computer Science and Engineering AGACSE 17, (2008)

Haruki, H., "A new functional equation characterizing generalized Joukowski transformations. Aequationes," Mathematica, Vol. 32, N° 2-3, PP. 327–335, (1987)

Katz J. and Plotkin A., "Low-speed Aerodynamics, From Wing Theory to Panel methods," New York, McGraw-Hill, (2015)

Malonek H. R; and Almeida R. D., "A note on generalized Joukowski Transformation," Applied Mathematics Letters, Vol. 23, PP. 1174-1178, (2010)

Merzbach U. C. and Boyer C. B., "A history of mathematics," John Wiley and sons. 3<sup>rd</sup> edition, (2011)

Nehari Z., "Conformal Mapping," Dover Publications, New York, (1982)

Paraschivou I., "Aérodynamique subsonique," Editions de l'Ecole Polytechnique de Montreal (Québec), Canada, (1998)

Ryhming I. L., "Dynamique des fluides," Presse polytechniques romandes, (2010)

Ralston A. and Rabinowitz P., "A First Course in Numerical Analysis," McGraw-Hill Book Company, (1985)

Suenaga K. and Sakai M., "A cubic spline approximation of an offset curve of a planar cubic spline," International Journal of Computer Mathematics, Vol. 78, N° 03, PP. 445-450, (2001)

UIUC Applied Aerodynamics Group, [http://www.ae.illinois.edu/m-selig/ads/coord\\_database.html](http://www.ae.illinois.edu/m-selig/ads/coord_database.html), department of Aerospace Engineering, College of Engineering, University of Illinois at Urbana, Champaign, Il, (2013)

Vinokur M., "On one-dimensional stretching functions for finite-difference calculations," Journal of Computational Physics, Vol. 50, N° 02, PP. 215-234, (1983)

Wang Z. and Wang K. A. S., "Cubic B-Spline Interpolation and Realization," In: Liu C., Chang J.,

Yang A. (eds) Information Computing and Applications. ICICA 2011. Communications in Computer and Information Science, vol 243. Springer, Berlin, Heidelberg, (2011)

## NOMENCLATURE

$\tau$	Airfoil trailing edge angle
$m$	Number of the points on the ellipse boundary
$Q_1, Q_2$	Constants for the stretching function
$\varepsilon$	Calculation error
$C$	Airfoil chord
$t_{\max}$	Maximum airfoil thickness
$\xi, \eta$	Position of a point on the ellipse boundary
$x, y$	Position of a point on the airfoil boundary
$n$	Power in the conformal mapping
$z_1$	Internal critical point in the airfoil plane
$z_2$	LE critical point in the airfoil plane
$\lambda$	Conformal mapping value
$\alpha, \theta, \varphi$	Angles in an airfoil triangle
$\Delta$	Angle that the segment connecting critical points 1 and 2 makes with the horizontal
$a_1, a_2$	Length of the triangle sides in the airfoil plane
$a, b$	Horizontal and vertical ellipse radius
$\mu$	Ratio $b/a$
$z$	Complex number in the airfoil plane
$\zeta$	Complex number in the ellipse plane
$\gamma_A$	Angle that makes the line joining the ellipse center and the TE with the horizontal
$\gamma_B$	Angle that makes the line joining the ellipse center and the LE with the horizontal
$a_{12}$	Distance between the two critical points 1 and 2
$\xi_C, \eta_C$	Ellipse center position
$\delta$	Angle of the discretization in the ellipse plane
$m_E$	Number of points on the airfoil upper surface
$m_I$	Number of points on the airfoil lower surface
LE	Leading edge
TE	Trailing edge
$M$	Mach number
$\alpha$	Incidence angle
$T$	Stagnation temperature
$P$	Pressure
$C_D$	Drag coefficient
$C_L$	Lift coefficient
$C_M$	Pitching moment coefficient
$j$	Complex number $j^2 = -1$
arg	Argument of a complex number
$N$	Iteration number for the dichotomy method
$V_i$	Tangential velocity at the control point
$q_i$	Source values at control points $i$ .
$g_i, h_i$	Control point position $i$
$u_i, v_i$	Horizontal and vertical component of $V_i$
$r_{i,j}$	Distance between control point $i$ and node $j$
$\beta_{i,j}$	Angle subtended by panel $j$ at control point $i$
$\theta_j$	Angle between segment ( $j$ ) and the horizontal
$\Gamma$	Value of the vortex intensity.
$f_1, f_2$	Functions for open air parameters
CFD	Computational Fluid Dynamics

## Indices

$i$	Counter on the boundary points
0	Stagnation condition
$\infty$	Upstream Condition